ATLAS NOTE

July 8, 2014

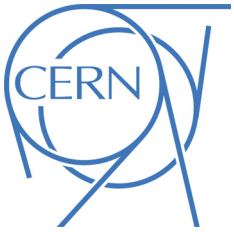

Test of a resistive micromega v 3.0 prototype with VMM1 readout using $\geq$ 0.8 GeV/c^2 cosmic muons

K. DiPetrillo[a], N. Felt[a], M. Franklin[a], P. Giromini[a,b], J. Guimarães da Costa[a], T. Lazovich[a], H. Skottowe[a], B. Tong[a]

[a]*Harvard University, Cambridge, Massachusetts 02138, USA*
[b]*Laboratori Nazionali di Frascati, Istituto Nazionale di Fisica Nucleare, Frascati, Italy*

Abstract

We present a detailed study of the VMM1 readout electronics using a resistive micromega v3.0 prototype and cosmic muons.

1 Introduction

This is our fourth note on the performance of resistive micromega detectors and the VMM1 readout electronics. In the previous notes [1, 2, 3], we used signals produced by ^{55}Fe decays. Paraphrasing the sequel *Games of Thrones*, this time we, the wildlings beyond the Wall, use cosmic muons to expose the *good deeds* of the King's hands Vinnie of BNL and Rui of CERN. The cosmic ray telescope is described in Section 2. Sections 3 and 4 describe the micromega prototype v 3.0 and the calibration of the VMM1-based readout system, respectively. The response of the detector to cosmic muons is presented in the next sections which are followed by a concise conclusion.

2 The cosmic-ray telescope

The Harvard cosmic ray telescope (HCRT), shown in Fig. 1, has been built in 2013 and commissioned during the Winter of 2014. It consists of two hodoscopes separated by 2.5 m and interleaved with a

Figure 1: The Harvard cosmic ray telescope (HCRT), described in Sec. 2.

concrete block 5 feet thick. Each hodoscope consists of 6 scintillator counters, 20 cm wide in the y direction (covering from y=-60 to y=60 cm) and 200 cm long in the x direction. Each scintillator is read by two photomultipliers at its ends. We use the time difference between the two photomultipliers of each counter to reconstruct the x-coordinate of a muon [1]. The trigger is defined by the coincidence of four signals corresponding to one counter on the bottom and one of the top layer. When a trigger arrives,

[1] We have measured $x = 6.28$ (cm/ns) $\times \Delta t$ (ns), where Δt is the time difference between the photomultiplier signals. The RMS x resolution is $\simeq$ 15 cm. The y resolution is $20/\sqrt{12} = 6$ cm.

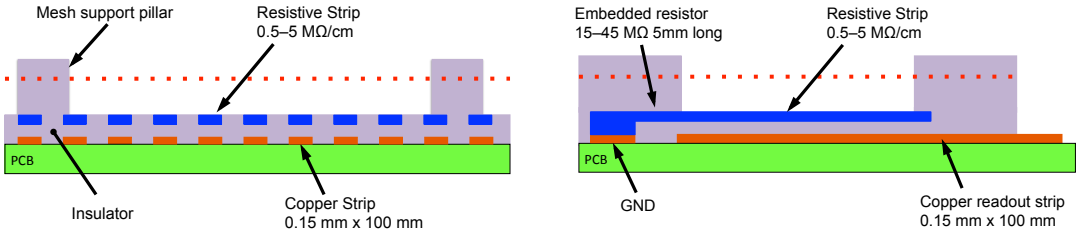

Figure 2: Sketch of micromega resistive and readout strips from the NSW TDR [5] . The width and pitch of the strips has changed (see text).

the time distance between the signal of each counter and the trigger is measured using a Lecroy 3377 multi-hit TDC, which has a 0.15 ns resolution, and subsequently acquired with a CAEN 111C camac crate controller.

The micromega detector is positioned on top of the concrete block with the readout strips parallel to the x axis. The micromega center is at (x, y)=(0,0). Since its size is 10×10 cm^2, we have added one scintillator counter of the same size, referred to as SP (small pad), on top of the micromega detector. The SP counter is also read out by two photomultipliers on opposite sides. We also require signals from the SP counter to generate a trigger. A trigger starts the readout of the CAMAC crate and of the VMM1 chip containing all micromega signals arrived at least 900 ns before the trigger. The arrival time of the micromega signal is compared to that of the SP counter which has a 1.2 ns resolution. Offline we remove those events in which there are more than two TDC hits on each of the three scintillator planes; this requirement removes approximately 10% of the events in which the muon is accompanied by a shower of other particles. In this configuration, the telescope accepts muons with energy ≥ 0.8 GeV/c and with polar angle as large as $\pm 20^\circ$ with respect to the vertical direction. The average muon angle of incidence is 90° with a RMS deviation of $\pm 9^\circ$ in the $y-z$ plane perpendicular to the micromega strips. More details about the HCRT performance can be found in Ref. [4].

3 The v 3.0 resistive micromega prototype

The micromega prototype v 3.0, a sketch of which is shown in Fig. 2, is built according to the NSW TDR specifications [5]. The amplifying gap is 128 μm thick. The cathode is a woven stainless steel mesh with 400 lines/in and a wire thickness of 18 μm. The mesh is kept at the 128 μm distance from the anode by a matrix of Pyralux pillars with 400 μm diameter and spaced by 2.5 mm in the x and y direction. The anode consists of resistive strips 15 μm thick deposited on a 50 μm thick Kapton foil. The resistive strips are 100 mm long in the x direction, 200 μm wide, and with a 400 μm pitch. The resistance of each strip is 5 MΩ/cm. Each resistive strip is connected to ground with a 45 MΩ resistor. The resistive layer is built on top of the readout electrode. The electrode consists of 17 μm thick copper strips, 300 μm wide, with a 400 μm pitch and 10 cm long in the x direction. The 5 mm drift gap is built on top of the amplifying gap.

For these measurements, we use a 93% Ar + 7% CO_2 gas mixture. Voltages are supplied by a CAEN DT5221 HV power supply. The mesh is at ground, the resistive anode, stabilized with a 100 nF capacitance, is set around 550 V. The drift voltage is set at -200 V and filtered with a RC circuit with a 100 ms time constant. As shown by Fig. 4, for drift voltages higher than 200 V, the mesh becomes less transparent.

In Refs. [1, 3], we did report that the breakdown voltage of amplifying gaps with grooves between anode strips was a function of the radiation exposure. The reason was tracked by Rui De Oliveira to pollution in the grooves that could not be burned by applying HV to the chamber filled with air. This

prototype went through extreme cleaning [6], and its breakdown voltage (570 V) does not depend on the radiation intensity.

As a benchmark, we have measured the ^{55}Fe charge collected by all x strips with an ORTEC 142C charge preamplifier followed by a ORTEC 472A shaping amplifier set to a 1 μs shaping time. Figure 3 shows the ^{55}Fe spectrum at 540 V. Figure 4 shows the charge corresponding to the 6 KeV peak as a function of the anode voltage.

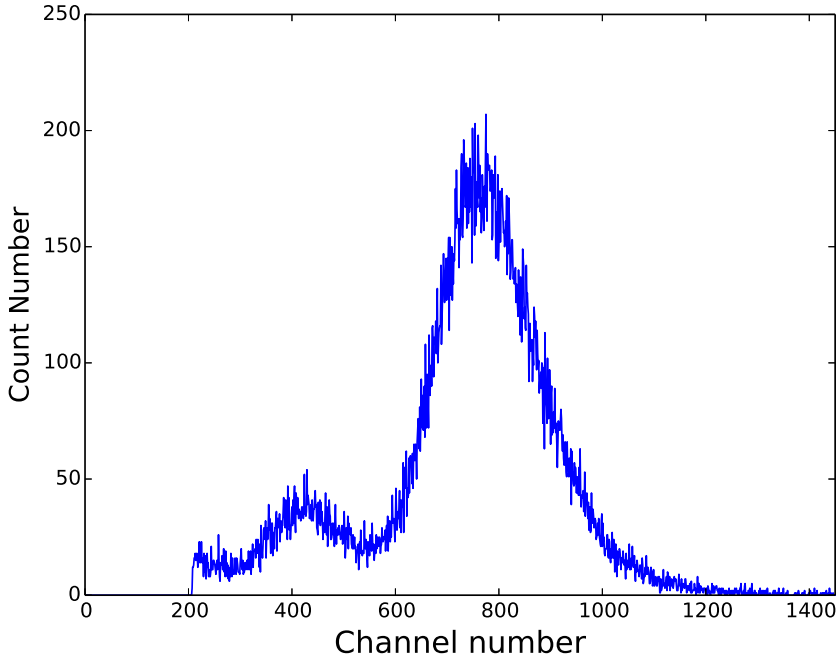

Figure 3: Charge distribution of the signals due to ^{55}Fe decays using an ORTEC 142C charge amplifier followed by an ORTEC 472A shaping amplifier with 1 μs shaping time.

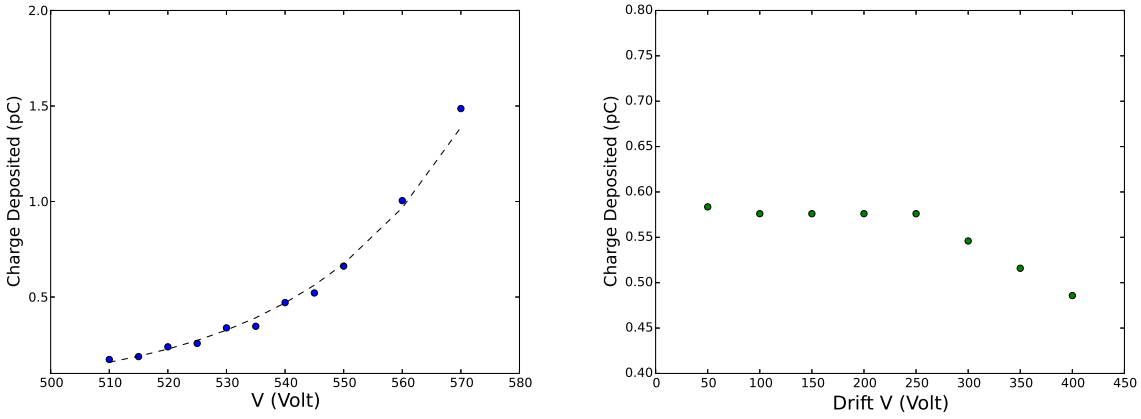

Figure 4: Dependence of the ^{55}Fe 6 KeV peak on the anode (left) and drift (right) voltage.

4 The VMM1 readout

In these measurements, we use two VMM1 chips covering the central 5.12 centimetres of the micromega. In the following, we use the convention that the number of the 128 strips increases with increasing y value. The FE-mini1 board hosting the first 64 strips is referred to as board-0 or board-16, whereas the next is referred to as board-1 or board-17. The functionality of the VMM1 is detailed in Ref. [8]. For each channel, the ASIC chip contains an analog section with a selectable-gain charge preamplifier and a high-order DDF (Delayed Dissipative Feedback) shaper with a shaping time selectable from 25 to 200 ns [2]. We have used the largest gain of the charge amplifier (9 mV/fC) because a significant fraction of MIP signals is close to the discriminator threshold. We have studied the chip performance using 100 and 200 ns shaping times.

The shaping amplifier is followed by a discriminator with a threshold value common to all channels. The possibility is provided to adjust individually the threshold of each channel with a full range of 15 mV. As is well known, this fine adjustment is at the moment insufficient [3].

The output of the shaping amplifier is followed by a peak detector – armed by the discriminator – the voltage output of which, referred to as the PDO, is stored until digitized. The option is available for any channel over threshold to enable the acquisition of its neighbor channels. However, we find that the arrival time of neighbor-enabled signals is likely compromised by cross-talk in the chip, and this study does not use this option.

The detection of a peak starts the TAC ramp for this channel. All TAC ramps are stopped by the cosmic-ray trigger. The scale of the TAC ramp is selectable and we use 1 mV/1 ns. The TAC voltage, referred to as TDO, is also stored until read out together with the PDO and the channel address. Upon a trigger arrival, the stored PDO and TDO values are multiplexed to the BNL CDAQ card where they are digitized and transmitted together with the address of the channel. Data are recorded with a QT-based program [7]. We have not yet studied directly the performance of the ART signal, but we get a feeling of it, when generated at peak-finding, by looking at the time distribution of the earliest TDO signal in both FE boards.

4.1 VMM1 calibration

The VMM1 chip offers the possibility of calibrating the gain and pedestal of the PDO and TDO values. This is achieved by enabling a 1.2 pF test capacitor for each channel. A voltage step, controlled by the onboard pulser DAC and test clock, is sent to any combination of enabled channels. We measure the PDO pedestals and gains (mV/fC) of all 128 channels, one at a time, by using voltage steps generated with different DAC values (from 250 to 400 in steps of 50). As is well known, voltage steps do not correspond exactly to the DAC values and have been measured with an oscilloscope using the monitor channel. The relationship between DAC value and step voltage is quite different for the two chips. Figure 5 shows the calibration of the DAC pulse on each VMM1 chip. In the Atlas experiment, each DAC output will have to be measured with accurate digitizers or the calibration will be a never ending loop.

The TDO values have been calibrated using DAC=400 step pulses and delaying the TAC stop by 250, 500, 750 and 1000 ns with respect to the injected-pulse time. Figures 6 and 7 show intercepts and slopes of the time and charge calibration for each of the 128 VMM1 channels. We have calibrated one channel at a time because it is well known by now that the leakage rate of the VMM1 multiplexer can be as large as 1.0 mV/μs, and the calibration would depend on the number of channels fired at the same time. To mitigate this problem, we digitize only once the TDO and PDO values of each channel. For data events with more than one strip signal in each ASIC, we correct for the measured leakage rate as detailed in Ref. [3].

[2] The analog output of the shaping amplifiers can be monitored one channel at the time.

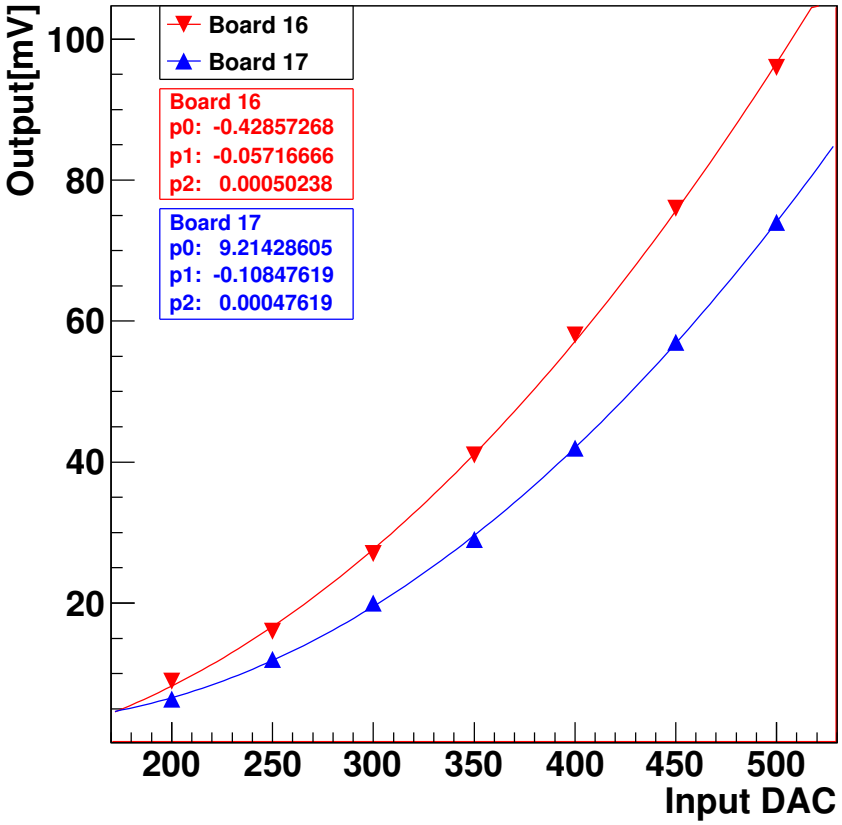

Figure 5: Calibration of the test pulse DAC of each of the two VMM1 chips. The lines and statistics insert show a quadratic fit to each set of points.

4.2 VMM1 thresholds

The same DAC value of 250 sets the common discriminator threshold at 258 and 215 mV in board-16 and board-17, respectively. As seen in the previous figures, pedestals are also quite different. Therefore, we have set the threshold of each channel by using data to equalize the minimum charge detected by each strip. The best equalization is shown in Fig. 8. It is obvious that there are signals close to the threshold and likely below it.

4.3 Neighbor channel enable

Therefore, it seemed a good idea to use the neighbor-enable option to recover signals under threshold. Figures 9 show the TDO distribution for each channel in 50000 muon events acquired using or not-using the neighbor-enable option. One sees that channels rescued as neighbor arrive approximately 100-150 ns earlier than channels above threshold. Since, as we will see later, the electronic noise is negligible, this effect has to be caused by cross-talk inside the ASIC. In any event, we decided not to use this option in the remaining of our study.

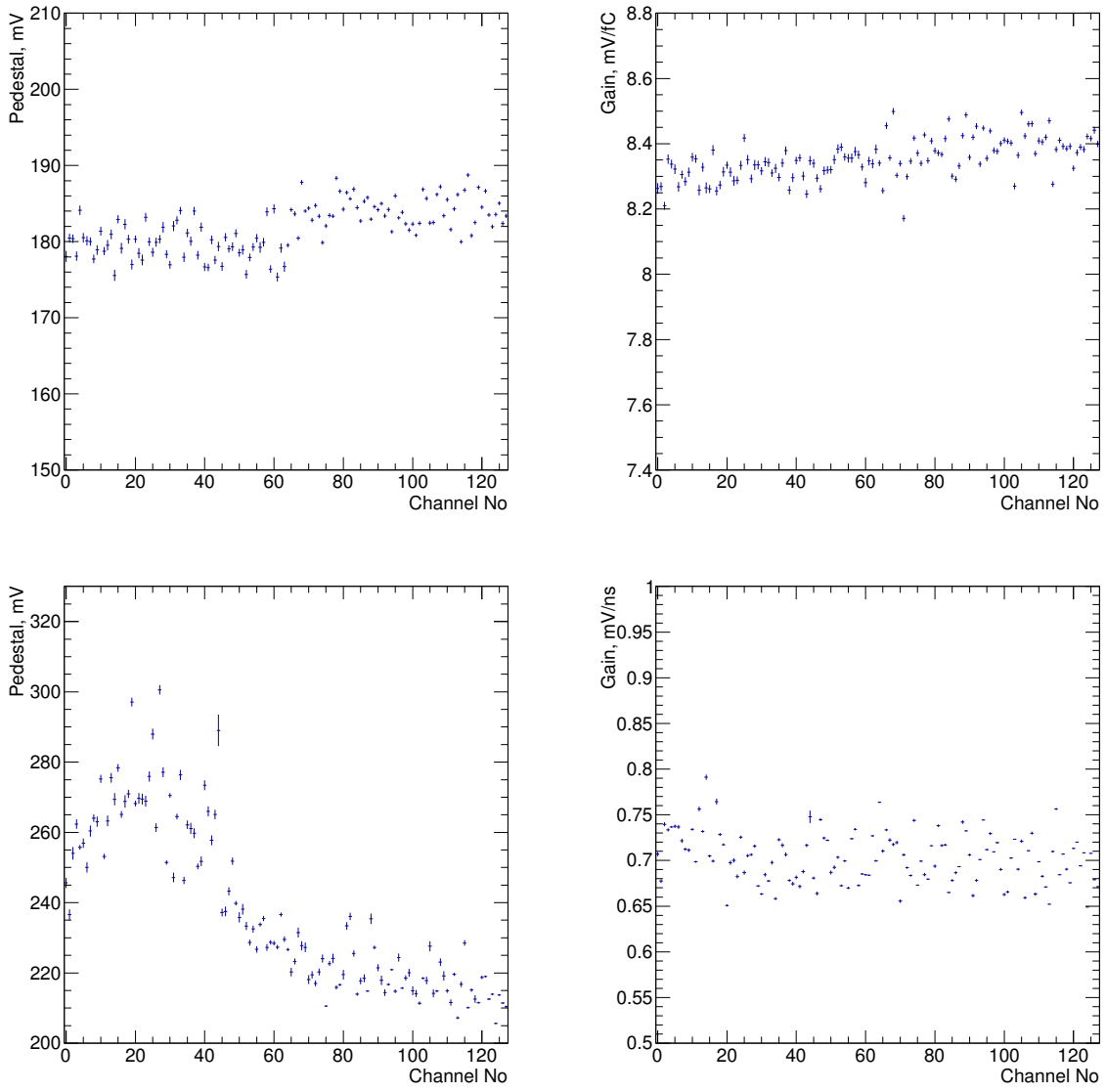

Figure 6: Results of the calibration of the two VMM1 chips when using a shaping time of 200 ns. Pedestals (top left) and Gains (top right) of the charge calibration. Pedestals (bottom left) and Slopes (bottom right) of the time calibration.

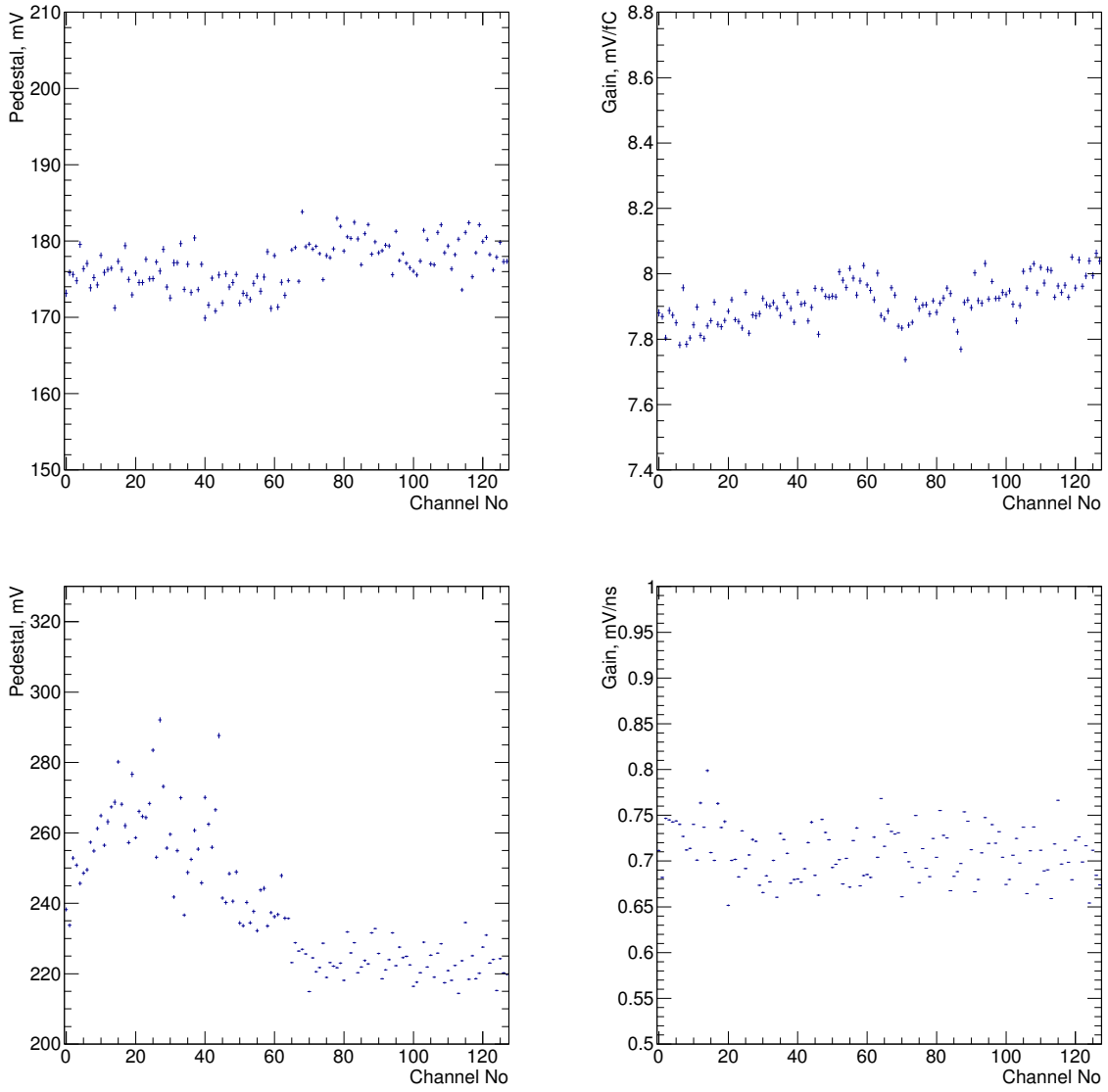

Figure 7: Results of the calibration of the two VMM1 chips, using a shaping time of 100 ns. Pedestals (top left) and Gains (top right) of the charge calibration. Pedestals (bottom left) and Slopes (bottom right) from time calibration.

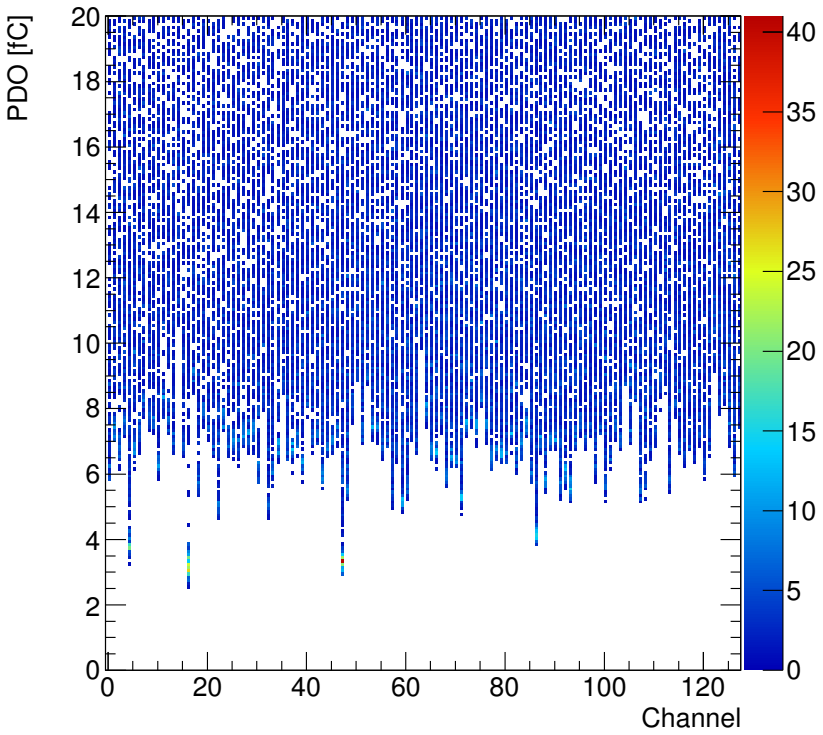

Figure 8: Charge deposited in each strip by 10^5 muons after a series of coarse and vernier threshold adiustments.

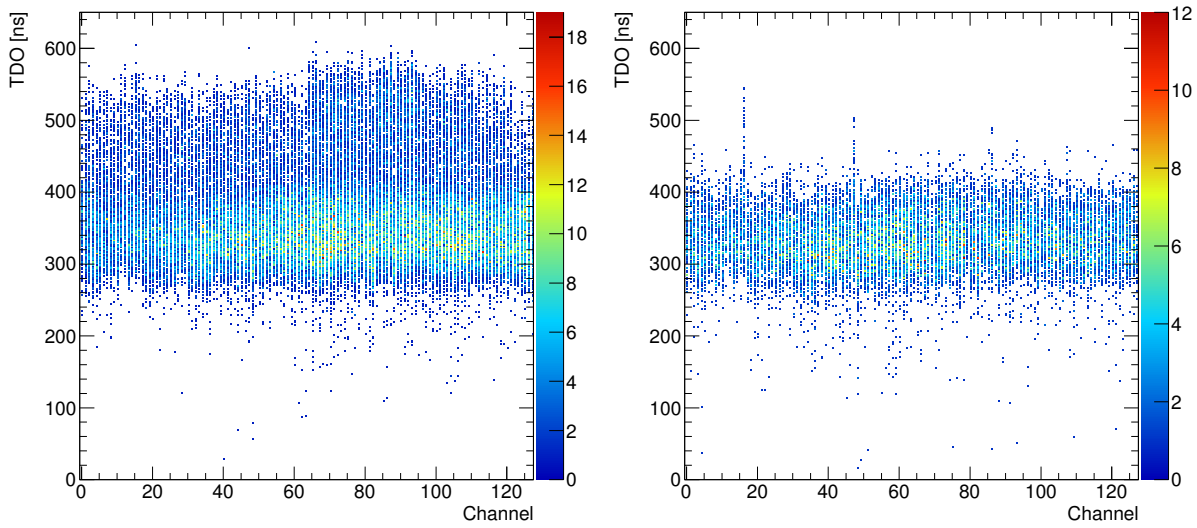

Figure 9: Distributions of TDO values for each channel in 10^5 muon events acquired using (left) and not using (right) the neighbor-enable option. The TDO value is the time difference between the micromega signal at peak and the cosmic trigger. Larger TDO values correspond to earlier signals.

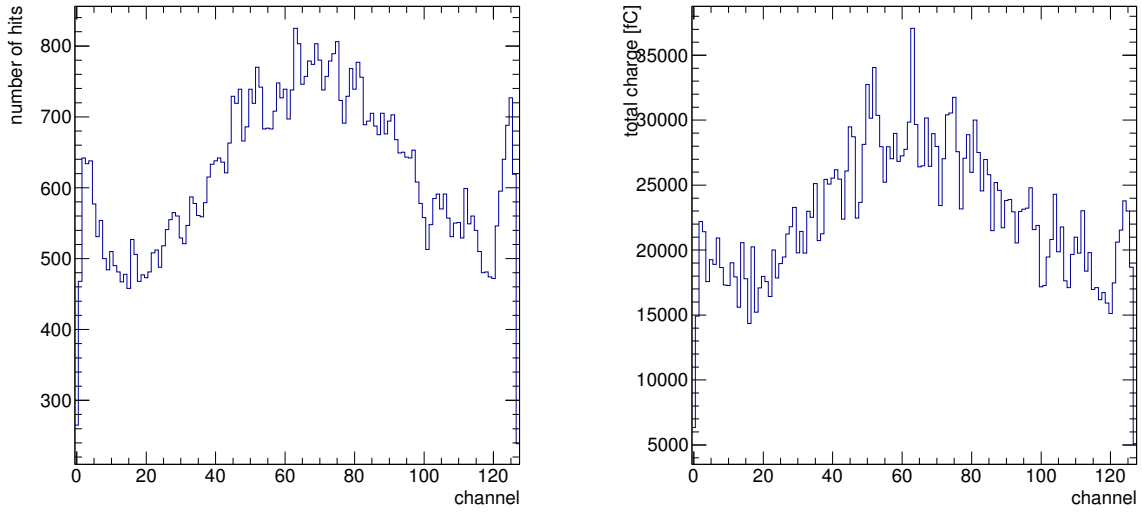

(a) (b)

Figure 10: Distribution of the number of hits (a) and deposited charge (b) in the 128 channels of the micromega readout for 25634 muon events, using a shaping time 200 ns and an anode voltage of 550 V.

5 Micromega response to cosmic muons

Figure 10 shows the number of hits and the total deposited charge for each readout strip in a run using a shaping time of 200 ns and an anode voltage of 550 V. The data set contains 86462 events with only one muon, 25634 of which leave a signal in the micromega detector [3]. The increase of counting rate and deposited charge in the first and last eight channels is due to muons passing close to but outside of the micromega area being readout. In some cases, we will apply a fiducial cut which excludes this region.

We use a simple cluster algorithm to reconstruct the muon position and arrival time using the readout strip signals. We sort all the hits according to their global strip number from 1 to 128. The clustering starts from the lowest strip with charge above 6 fC (seed). We then add to the cluster strips with higher strip number if their charge is larger than 2.5 fC and their arrival time is within the expected time window with the condition that their distance is smaller than or equal to five strips. Each time we add a strip, we update the end of the cluster, the total charge and the average arrival time. The same search is repeated from the last included strip. The same search is then extended backward starting from the seed strip. Strips not included in the first cluster are searched again for additional clusters. This algorithm reconstructs a cluster in 25589 events, 99.8% of all events with some deposited charge above threshold. The number of events with more than one cluster is about 3%, and to make life simple we use only the cluster with the highest charge unless specifically noted.

Figure 11 shows the charge distribution of reconstructed clusters. One notes that the charge integrated by board-16 is larger than that of board-17. This happens because its effective shaping time is larger. This difference cannot be detected during calibrations because, in contrast with micromega signals, step pulses have a risetime much smaller than the shaping time of the charge integrator. Accordingly, it will be shown later that TDO values generated at peak-found are smaller in board-16.

It is interesting to note that the average charge of the muon cluster is approximately 100 fC, or 1/6

[3] Because the effective area of the SP counter is difficult to assess, the fraction of events with a micromega signal cannot be translated into an efficiency measurement. However, this fraction can be used to monitor the dependence of the micromega efficiency on voltages and shaping times.

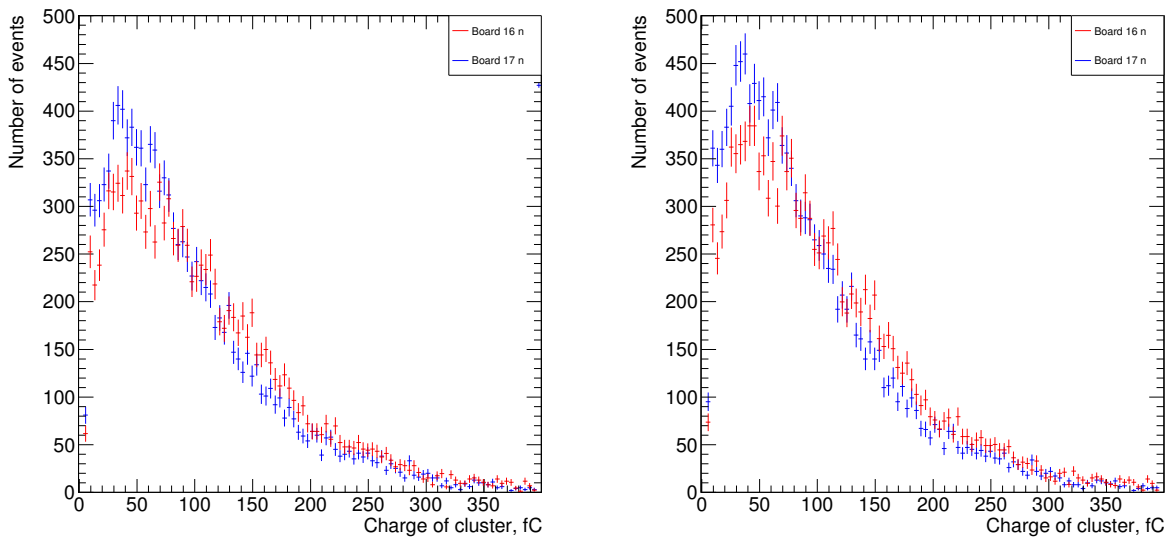

(a) (b)

Figure 11: Distribution of the charge of clusters reconstructed in board-16 and -17 with (a) and without (b) fiducial cut (see text), using a shaping time of 200 ns and an anode voltage of 550 V. Distributions are normalized to the same number of events.

of the charge corresponding to the 6 KeV peak integrated by a single ORTEC amplifier connected to all readout strips (see Section 3) [4]. One also notes that the charge distribution is close to the threshold which makes it difficult to assess the micromega efficiency with the present setup. As shown by Fig. 12, the small charge clusters are those with low strip multiplicity.

Figure 13 shows the distribution of the number of strips in reconstructed clusters. It also shows that all strips in a cluster are contiguous in more than 90% of the cases. Figure 14 shows the average charge of a cluster as a function of the number of strips in the cluster. In 98% of the clusters, i.e. those with $\leq$ 5 strips, the number of strips is linearly proportional to the collected charge. This is somewhat at odds with the popular model in which the strip multiplicity depends on the angle of incidence of a track. If this were the case, the average charge would be almost independent of the cluster multiplicity. This observation fits better a model in which: a) the drift of ions in the amplifying gap builds a difference of potential $\delta V(t)$ on the resistive anode; b) the strip signals arise from the capacitive couplings between the resistive anode and the readout strips; c) the larger is $\delta V(t)$, the larger is the number of strips with an induced signal above threshold. This raises a concern on the possible use of micromegas equipped with VMM readout as μTPC detectors, which is further investigated in Sects. 5.5 and 6.

5.1 Measurement of the electronic noise

We have investigated if signals close to the VMM threshold are due electronic noise by moving the SP counter to the side of the micromega. The fraction of muon events with a micromega cluster above threshold decreases from 29.6% to 0.07%. The distribution of the cluster charge for the same number of muon triggers is compared in Fig. 15. It is our conclusion that the signals close to the threshold are due to real muons and the electronic noise is negligible.

[4] The MIP ionization loss in 5 mm of gas is approximately 1 KeV.

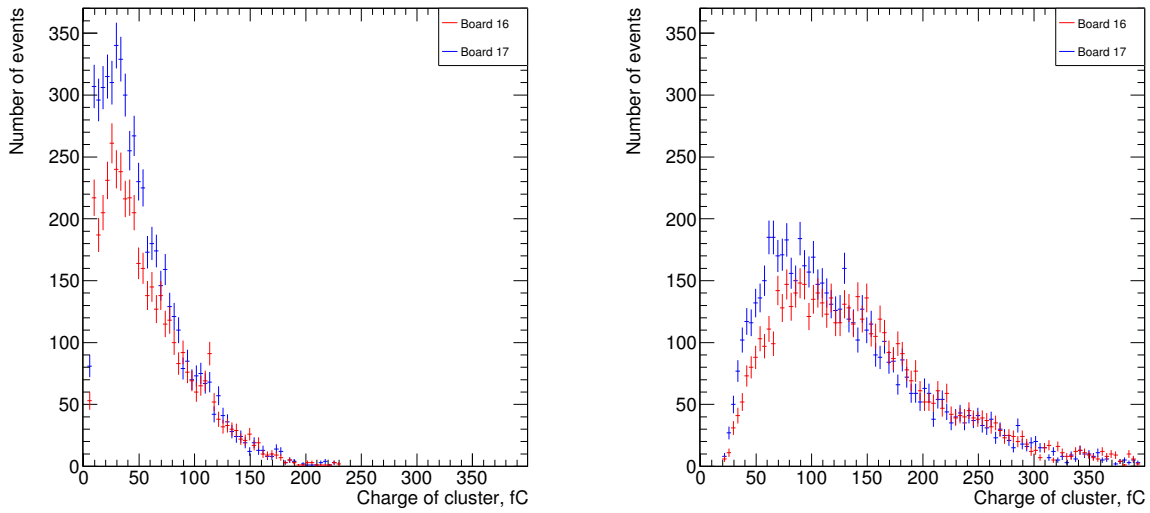

(a) (b)

Figure 12: Charge distributions of clusters consisting of (a) ≤ 2 and (b) ≥ 3 strips, using a shaping time 200 ns and an anode voltage of 550 V. The fiducial cut has been applied.

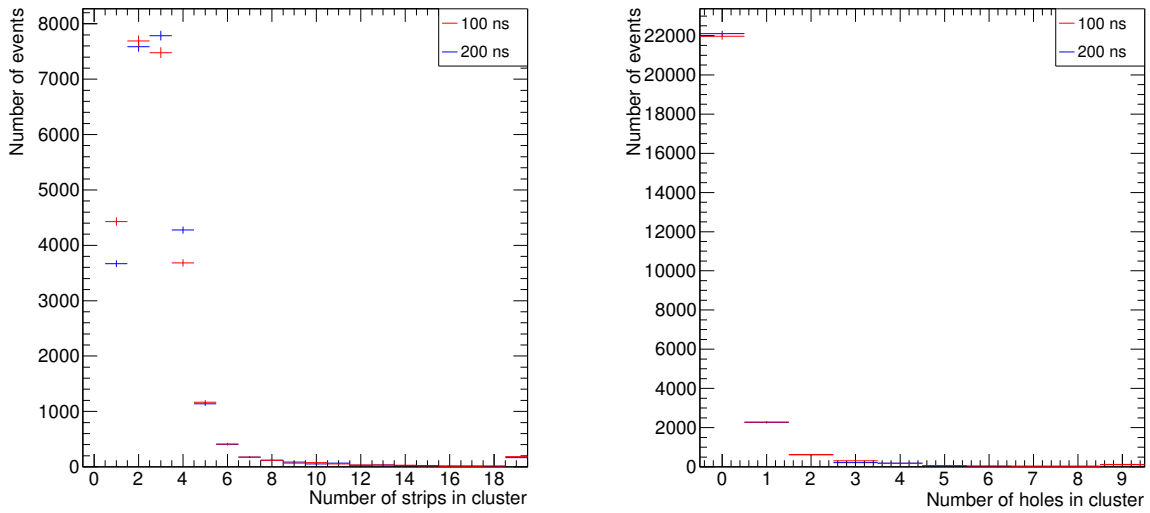

(a) (b)

Figure 13: Distributions of (a) the number of strips in a cluster and (b) of the number of missing channels inside a cluster, using an anode voltage of 550 V and shaping times of 200 ns and 100 ns.

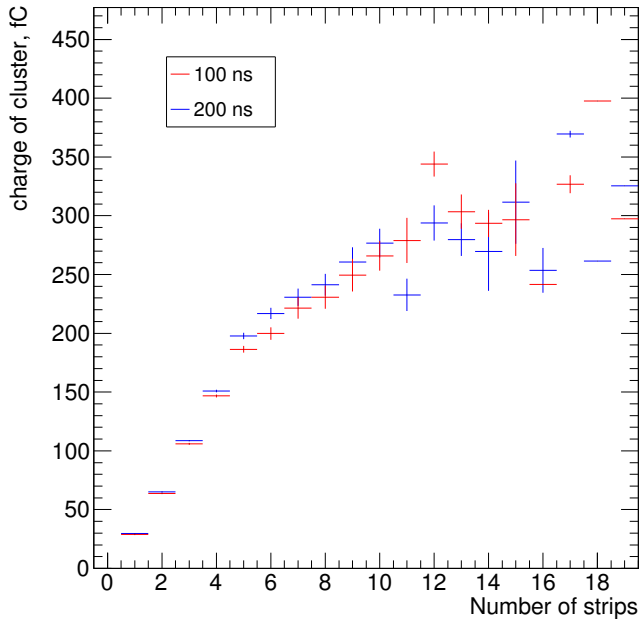

Figure 14: Average charge of clusters as a function of their strip multiplicity, using an anode voltage of 550 V and shaping time of 100 ns and 200 ns.

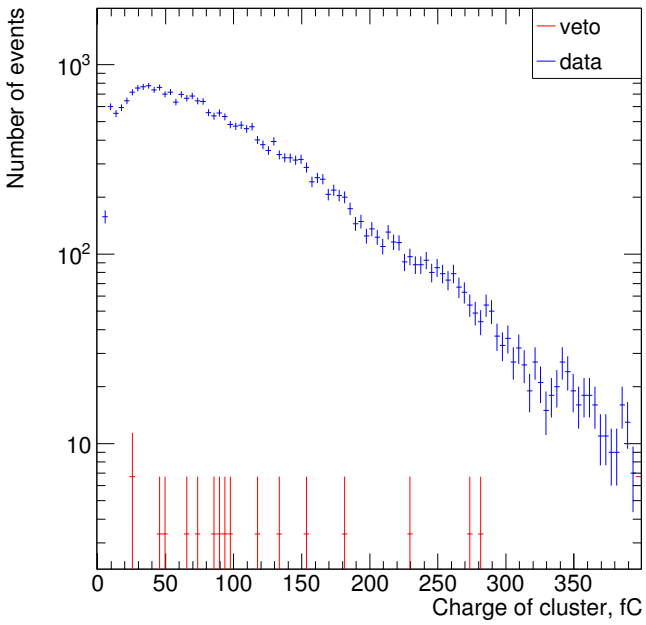

Figure 15: Distributions of cluster charges for muon events triggered with the SP counter on top (blue points) and to the side (red points) of the micromega. Distributions are normalized to the same number of muon triggers.

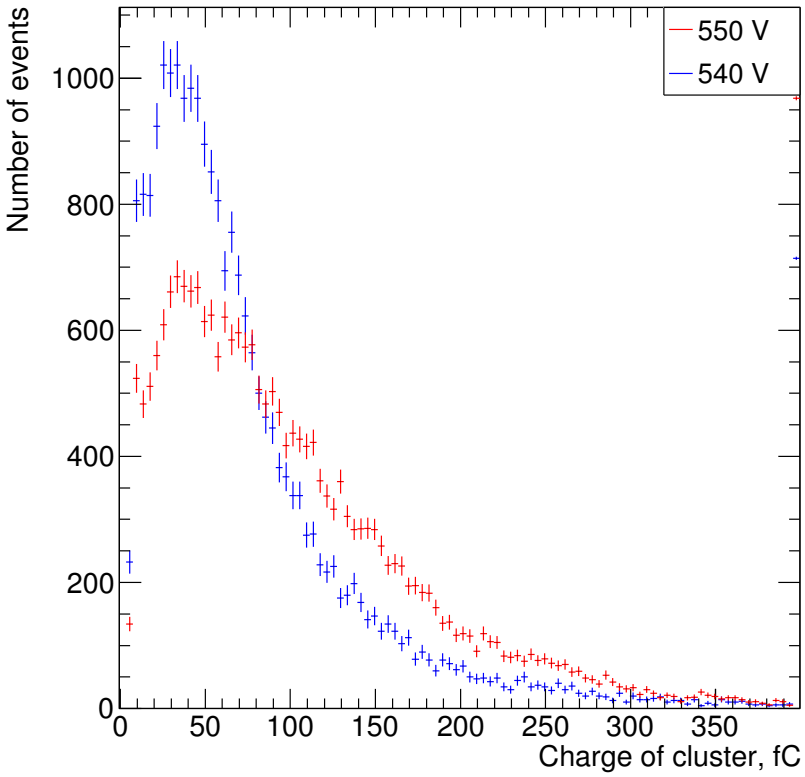

Figure 16: Distributions of the cluster charge for anode voltages of 540 and 550 V, using a shaping time 200 ns. The fiducial cut is applied.

5.2 Dependence of the collected charge on the voltage of the resistive anode

Figure 16 compares distributions of cluster charges when lowering the anode voltage from 550 to 540 V. The ratio of the averages of the cluster charge distributions is 72%, in reasonable agreement with the 68% expected from Fig. 4. However, the ratio of the number of reconstructed clusters normalized to the same numbers of muon triggers at 540 and 550 V is 1.007 ± 0.010. In conclusion, at 550 V the micromega efficiency is definitely in plateau.

5.3 Comparison between 200 and 100 ns shaping time

For triggering reasons, a shorter shaping time is often advocated. Using the 100 ns shaping time, we have collected 75874 muons events in which 20504 events have some micromega signal and in which 19964 events have at least one cluster. It follows that the micromega efficiency at 550 V drops by 11.2% when shortening the shaping time by 100 ns. Therefore, we see no point in exploring shorter shaping times. Figure 17 compares the cluster-charge distributions for 100 and 200 ns shaping times.

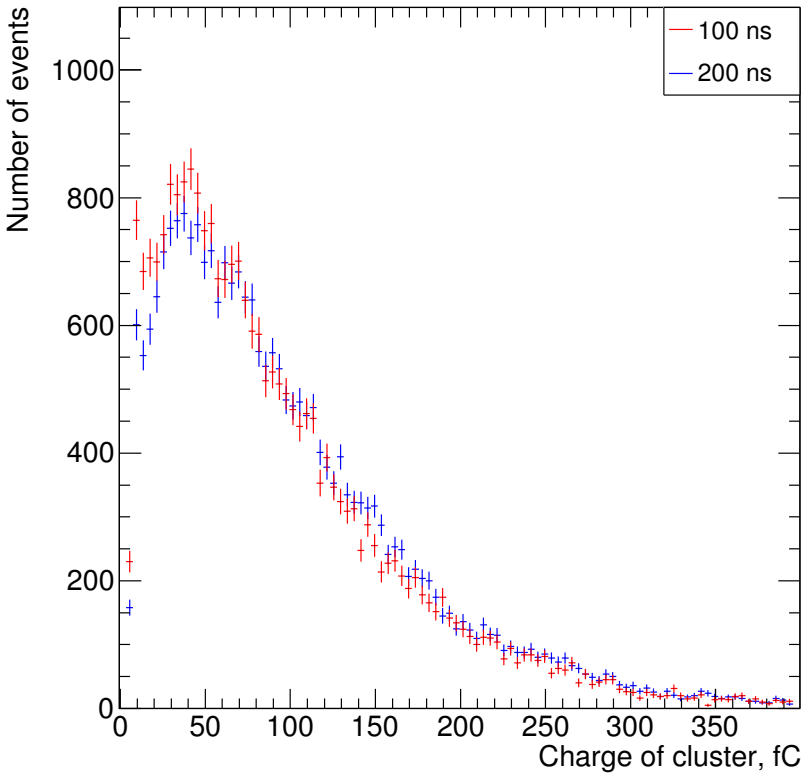

Figure 17: Distributions of the cluster charge using shaping times of 100 and 200 ns and an anode voltage of 550 V. Distributions are normalized to the same number of events. The micromega efficiency drops by 11.2% when using the shorter shaping time.

5.4 Arrival times of micromega signals

This subsection is dedicated to the accuracy of the VMM1 TDO values, defined as the time difference between an integrated micromega signal at peak and the SP signal which has an accuracy of 1.2 ns. When forming a cluster, we also average the TDO's of all strips belonging to the cluster, referred to as cluster-TDO. Independently of cluster finding, for every event we also calculate the largest, referred to as earliest-TDO, TDO value in the two VMM1 chips. This emulates the arrival time of the ART signal used by the micromega trigger.

Figure 18 shows the mean of the cluster-TDO's as a function of the cluster charge as well as the time distribution of all TDO's and earliest-TDO's for all channels. As mentioned earlier, board-16 has a longer shaping time and the cluster-TDO's arrive approximately 5 ns later. There is a small slewing of the arrival time as a function of the cluster charge, the slope of which is approximately 0.06 – 0.09 ns/fC. This slewing time is appreciable but negligible with respect to the RMS of the distribution of the cluster-TDO's shown in Fig. 19. This figure also shows the distribution of the earliest-TDO's in the event. One sees that the time jitter of the earliest-TDO covers at least 8 LHC bunches. This latter distribution is difficult to reconcile with that of the earliest arrival time based on a direct study of the ART signal [9] [5, fig. 5.9] unless the CDAQ card or the VMM1 chip introduce a random time jitter of the order of 100-150 ns between the cosmic trigger and the TAC stop. Figure 20 shows the earliest-TDO distributions for different track angles. Tracks with larger angles yields in average larger earlier-TDO's,

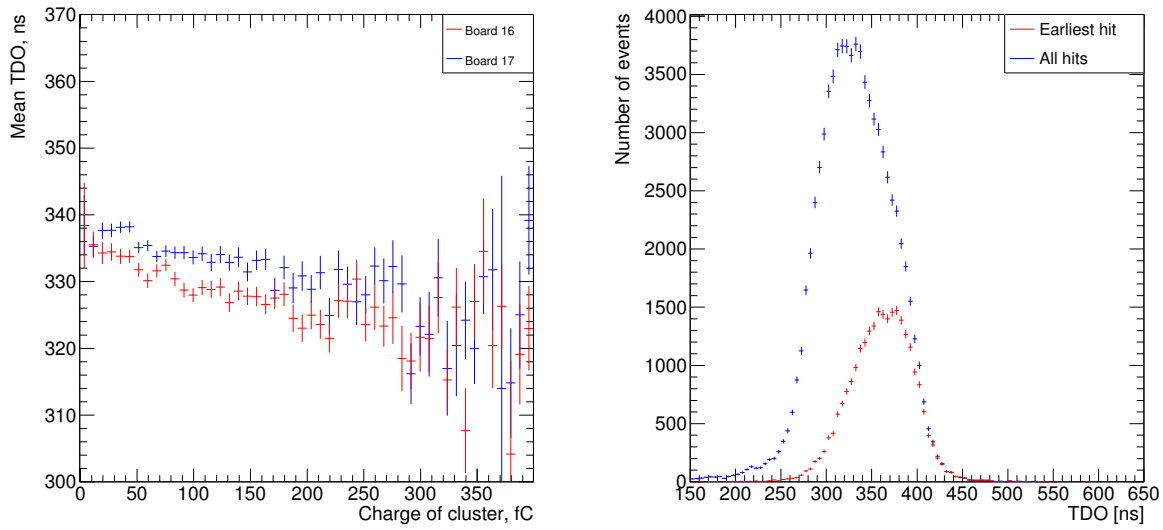

(a) (b)

Figure 18: (a): Mean of all cluster-TDO's as a function of the cluster charge for both VMM1 chips using a shaping time of 200 ns. The anode voltage is 550 V. (b): Time distributions of all TDO's and earliest-TDO's for all readut strips using the same settings.

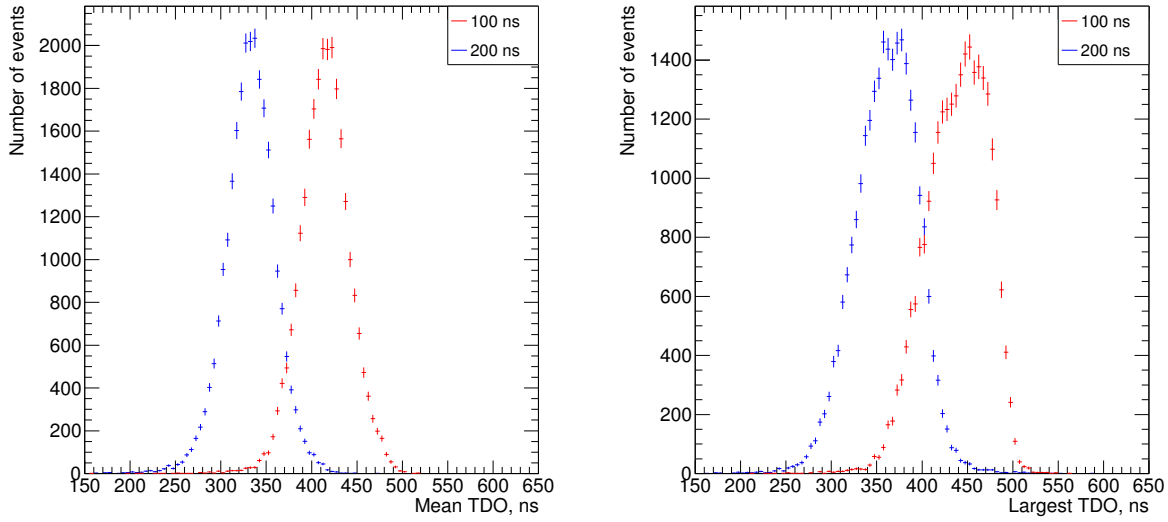

(a) (b)

Figure 19: Distributions of (a) the cluster-TDO's and (b) earliest-TDO's using shaping times of 100 ns and 200 ns and an anode voltage of 550 V. The 100 ns distribution is normalized to the same number of events as the 200 ns distribution.

but the overall time jitter ($\simeq$ 200 ns) is independent of the track's angle. The fact that the shape of earliest-TDO distribution depends on the track angle does not support the above-mentioned hypothesis that the width of the distribution is due to random jitter of the TAC stop in the VMM1 chip. We are presently adding the ART signals to our data acquisition system, and will revisit the issue in a not so distant future.

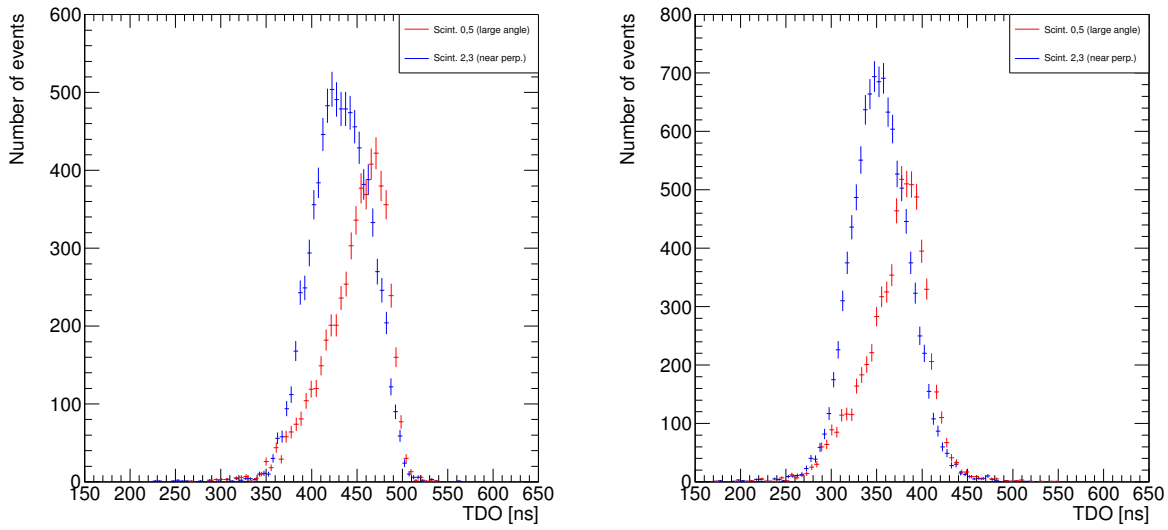

(a) (b)

Figure 20: Distributions of earliest-TDO for cosmic muon tracks passing through different bottom scintillators, using shaping times of (a) 100 ns and (b) 200 ns and an anode voltage of 550 V. Scintillators 0,5 (red points) correspond to track angles of 11°-16° in the y-z plane, whereas scintillators 2,3 (blue points) correspond to track angles of 0-5°.

5.5 Micromega response to the muon angle of incidence

We study the micromega response as a function of the muon angle of incidence by selecting muons triggered by different bottom scintillators with y coordinates ranging from −60 to +60 cm in steps of 20 cm. By requesting scintillator hits with increasing y-coordinate, we change the muon angle in the $y-z$ plane, orthogonal to the direction of the micromega readout strips, from −13° to 13° in five steps of 5°, each with an RMS of 1.5°. Figure 21 shows the y-position of micromega clusters, measured in strip number, as a function of y-trigger, the y coordinate of the bottom counter triggering the event. Figure 22 shows the average multiplicity of a cluster as a function of y-trigger. The average multiplicity increases by 0.6 strips when the muon angle of incidence increases from 0° to 13°. Ideally, the number of strips in a cluster should increase from 1 to 3 when the incidence angle grows from 0° to 13°. This does not happen because, as noted earlier, the cluster size is mostly determined by its charge.

6 Study of the μTPC mode

A detailed study of the micromega performance as μTPC [10] has shown that, when using the APV25 readout, it is possible to reconstruct angles of incidence with an accuracy of the order of 2-3°. Similar resolutions have been achieved using the VMM1 readout [11]. When using VMM1, the only additional information is the TDO value of each strip in a cluster. Therefore, we were puzzled by the latter result [11] since the cluster multiplicity depends mostly on the cluster charge. We are also puzzled that the reconstructed angle agrees with the real angle of incidence within a couple of degrees, as shown in Fig. 27 of Ref. [11]. In that measurement, the TDO's values are digitized 8 times, and not 1 time as in our case, and the measurement in Ref. [11] does not correct for the TDO voltage leakage while waiting to be digitized. According to our measurement [3], the TDO value of channel $n+1$, digitized after channel n, is reduced by 0.3%. Since the study in Ref. [11] uses a TAC scale of 500 ns, the time difference

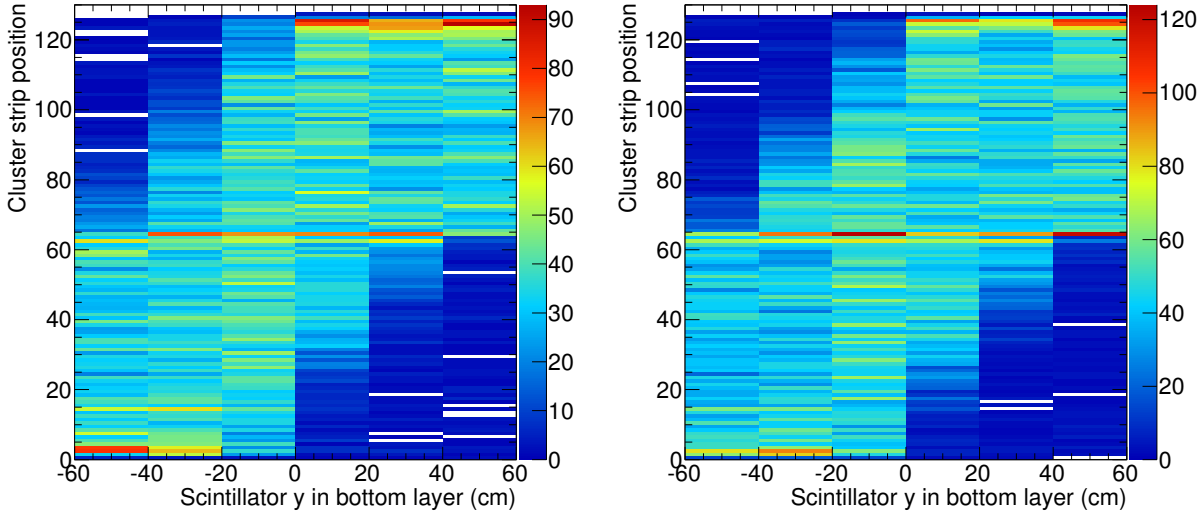

Figure 21: Dependence of the cluster y coordinate (measured in strip number) on y-trigger (see text) for 100 ns peak time (left) and 200 ns (right). The anode voltage is 550 V.

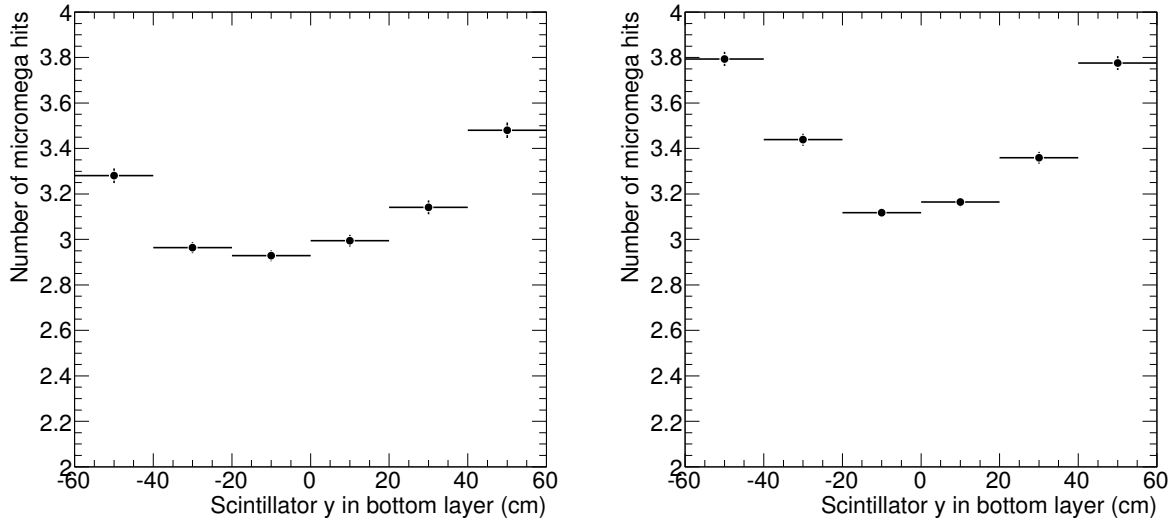

Figure 22: Average multiplicity of clusters as function of y-trigger for 100 ns peak time (left) and 200 ns (right). The anode voltage is 550 V.

between any two adjacent strips acquires a leakage-induced offset of $\simeq$ 1.5 ns. Using a drift velocity of 1 mm/20 ns, this non-corrected bias should have produced an offset of 10-11° between the reconstructed and real angles.

We put to use the quite large angular coverage of the HCRT to investigate further. In 44% of the events, the cluster multiplicity is ≤ 2 and, following Ref. [11], we do not attempt to reconstruct the track angle. The remaining 56% of the events are dominated by multiplicity 3, in which case no hits can be excluded by using tricks such as representations in Hough space [11]. For clusters with three or more strips we fit the TDO values of the strips with a straight line. In 20% of the cases (multiplicity larger

than 3), one could possibly improve the fit result by ignoring strips yielding a bad χ^2, but at this stage we do not see the point of showing better resolution for less than 20% of all events. The slope of the fit is converted into an angle of incidence assuming that the drift velocity of electrons is 1 mm/20 ns. In our convention, a nil slope (all hits at the same time) yields an incidence angle of 90°. Most fits return 50% uncertainties. Figure 23 shows the dependence of the angle of incidence reconstructed in μTPC mode on y-trigger. The angular resolution is approximately 43°. As a next step, we will try to improve the angular resolution by adjusting TDO errors and values as a function of the strip charge, but we do not expect an improvement of a factor of 10.

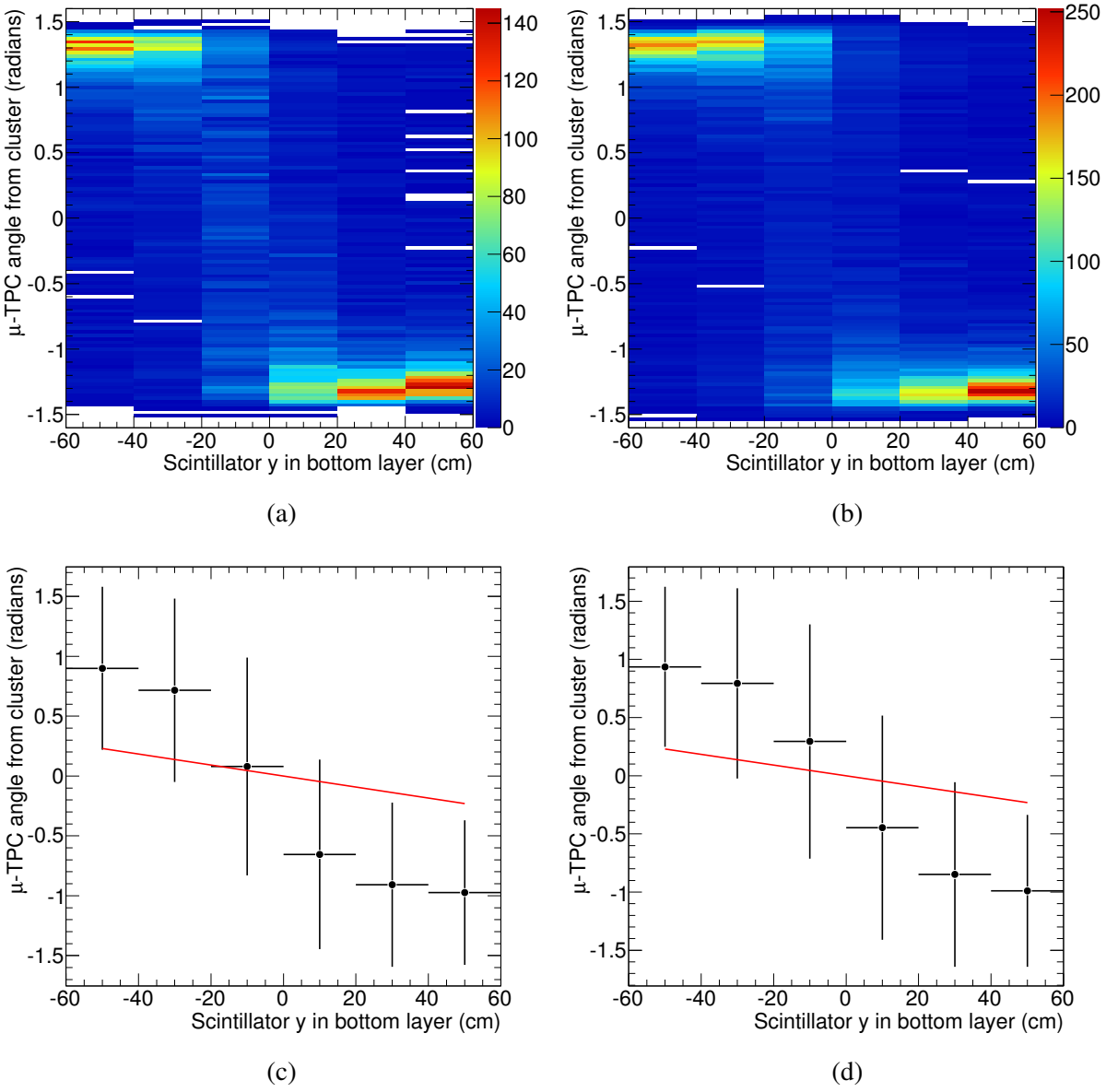

Figure 23: Distribution of track's angles of incidence, reconstructed in μTPC mode, as a function of y-trigger: plots (a) and (c) use a 100 ns shaping time, whereas (b) and (d) use a 200 ns shaping time; plots (c) and (d) are x-profile histograms of (a) and (b), respectively. The error bars represent the RMS deviation. The red line on the profile histograms indicates the actual track angle as function of y-trigger, with a maximum angle of $\pm 13° = \pm 0.23$ radians at $y = \mp 50$ cm.

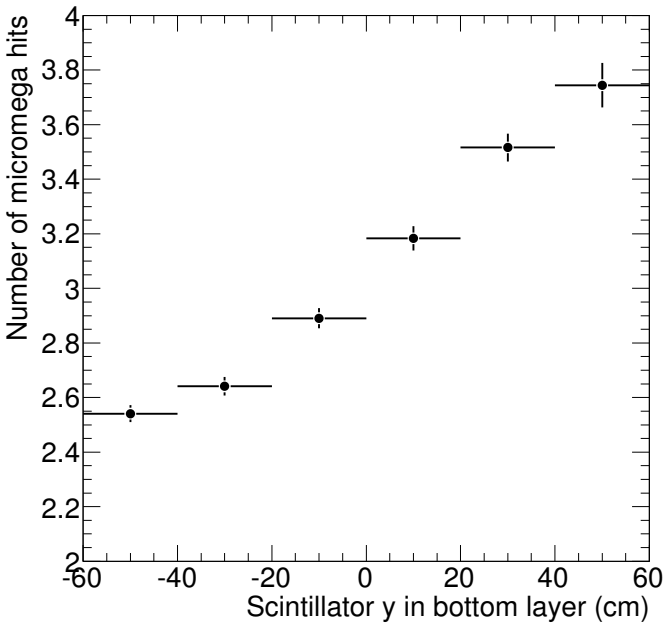

Figure 24: Average hit multiplicity of clusters as function of y-trigger using a 100 ns shaping time and an anode voltage of 550 V.

6.1 Study of tracks with angle of incidence as large as 25°

In this study we use a 100 ns shaping time and an anode voltage of 550 V. The center of the micromega detector and SP counter is moved from $y = 0$ to $y = -50$ cm. By requesting hits in bottom scintillator with increasing y-coordinate, we select muon angles in the $y - z$ plane, orthogonal to the direction of the micromega readout strips, from 0° to 25° in five steps of 5°, each with an RMS of 1.5°. We have collected 40024 single muon events, in which we reconstruct 11321 clusters. By comparing with Sec. 5.3, the micromega relative efficiency increases from 26.4% to 28.3% as tracks with higher incidence angle ionize a thicker layer of gas. The distribution of the average strip multiplicity of reconstructed clusters is shown in Fig. 24.

Figure 25 shows the average angle, reconstructed in μTPC mode, and its RMS deviation as a function of y-trigger for clusters with three or more strips and clusters with two strips only. Again, up to angles of 25° the average reconstructed angle using ≥ 3-strip clusters differs visibly from the real angle of incidence and the angular resolution is never better than 40°. The 2-strip cluster case is interesting because one should predict easily the RMS angular resolution. Since the RMS noise of each TDO, digitized only once, is about 2 ns, one would expect an angular resolution of about 20° when reconstructing track angles with 2-strip clusters, whereas ≃ 60° RMS is measured. In the future, we will study events collected with a smaller TAC scale to reduce the RMS noise in nanoseconds.

7 Conclusion

We present a detailed study of the performance of a micromega prototype v 3.0 equipped with VMM1 readout. We rediscover a number of known shortcomings, and a few problems which went undetected or overlooked when analyzing previous test-beam data. The study shows that a well-run and well-understood cosmic ray telescope is competitive with, if not superior to test beams, and it can be used to test in a few days the performance of the VMM2 readout whenever available.

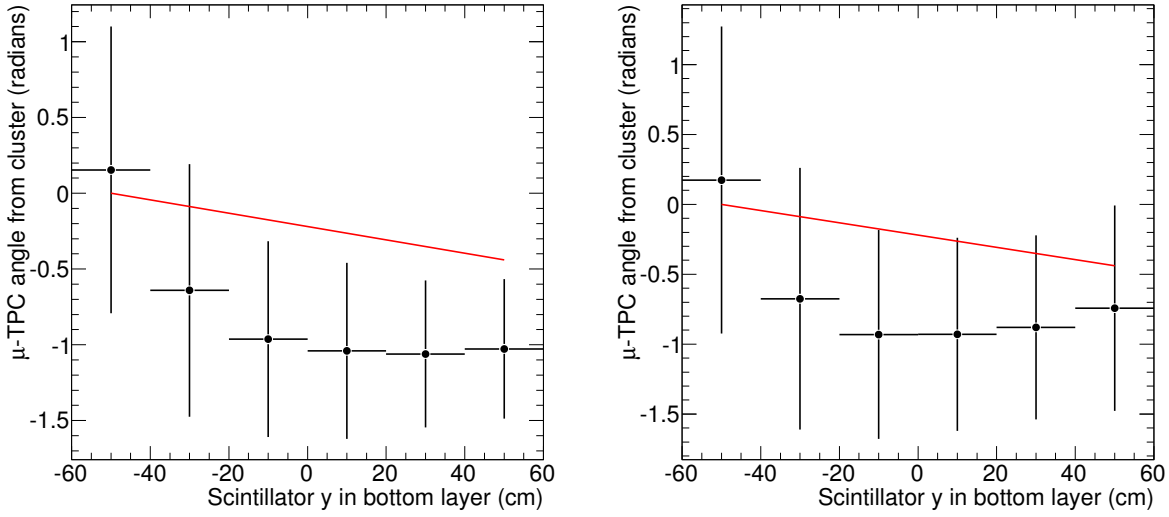

(a) (b)

Figure 25: Average track's angle of incidence, reconstructed in μTPC mode, as a function of y-trigger. (a) uses only clusters with at least 3 hits, whereas (b) uses only clusters with exactly 2 hits. The red line indicates the actual track angle as function of y-trigger, ranging from 0° at $y = -50$ cm, to $-25° = -0.44$ radians at $y = +50$ cm.

References

[1] J. Connors *et al.,* ATL-COM-UPGRADE-2013-019.

[2] J. Connors *et al.,* ATL-COM-UPGRADE-2013-023.

[3] J. Connors *et al.,* ATL-COM-UPGRADE-2013-034.

[4] H. Skottowe, `https://indico.cern.ch/event/316354/contribution/2/material/slides/`; J. Guimarães da Costa, `http://indico.cern.ch/event/298095/contribution/78/material/slides/`.

[5] ATLAS New Small Wheel Technical Design Report, ATLAS-TDR-020, CERN-LHCC-2013-006

[6] R. De Oliveira, private communication: "Usually only DI water with a high pressure spray (100 Bars) is enough. For your detector I've been obliged to dip it in a caustic soda bath at 20% concentration at 50deg during 5 min followed by a neutralisation bath of H_2O+H_2O_2+H_2SO_4 during 5 min + a high pressure DI water rinse. This treatment removes a thin skin of the Photoimageable coverlay."

[7] The QT based data-acquisition software was provided by G. Iakovidis, with our own modifications.

[8] More VMM1 details can be found at `https://twiki.cern.ch/twiki/pub/Atlas/NSWelectronics/VMM1_datasheet_v3a.pdf` by G. De Geronimo *et al.*

[9] V. Polychronakos, *Micromega trigger tests with MSW*, `https://indico.cern.ch/event/298095/session/4/contribution/77/material/slides/1.pdf`.

[10] T. Alexopoulos, *Highlights from 2013 test-beam analysis*, `https://indico.cern.ch/event/298095/session/4/contribution/60/material/slides/0.pdf`.

[11] T. Alexopoulos *et al.*, *Performance of the first version of VMM front-end ASIC with resistive micromega detectors*, ATL-COM-UPGRADE-2014-010